

# Influence of CaO on the Nanohardness Behaviour of AZ63 Magnesium Alloys Produced by Mechanical Alloying Method

M. BOZTAS, S. OZARSLAN AND O. SAHIN\*

Mustafa Kemal University, Science and Art Faculty, Micro/Nanomechanic Characterization Laboratory, Hatay 31034, Turkey

In this study we aimed to produce AZ63 magnesium alloys containing different amounts of CaO, to investigate the nanohardness behaviour of the resulting alloys. These alloys were produced by mechanical alloying under argon atmosphere. Magnesium based alloys with the initial CaO content of 0.1%, 0.3%, and 0.5% were produced by high-energy ball milling, followed by process that involved cold pressing and sintering. These alloys were characterized using scanning electron microscopy, scanning probe microscopy, X-ray diffraction, and nanoindentation methods. Unloading segments of nanoindentation curves were analyzed using Oliver-Pharr method. Experimental results show that measured nanohardness exhibits a peak load dependence. As a result, in these alloys the microstructure and nanohardness depend on the content of CaO.

DOI: [10.12693/APhysPolA.130.357](https://doi.org/10.12693/APhysPolA.130.357)

PACS/topics: 62.20.-x, 87.85.J

## 1. Introduction

Magnesium alloys (AZ91, AZ31, ZE41, WE43, AZ63, etc.) have a wide application area due to low strength-to-weight ratio, high mechanical, thermal and electrical properties [1]. Magnesium alloys were used in many areas such as automobile industry, commercial electronic devices, space technologies and biomedical applications [2]. Magnesium alloys have promising applications in biomedical sector because of their high biocompatibility and biodegradability properties [3]. In addition, magnesium does not have toxic effects when dissolved in the body. This is why magnesium alloys have been the preferred biomaterials during recent years [4]. Therefore, the development of new technologies to enhance mechanical properties of these alloys is very important for biomedical applications. Most of magnesium-aluminum alloys contain aluminum with small amounts of zinc. One of these, the AZ63 alloy, is the most extensively used magnesium alloy. The only existing phase in this alloy, which precipitates continuously and discontinuously, is the intermetallic  $\beta$ -phase ( $Mg_{17}Al_{12}$ ) [5].

Nanoindentation has been widely used for characterization of the nanomechanical properties of nanomaterials [6], and thin films [7, 8], because of its high sensitivity and the excellent resolution for obtaining the nanohardness, elastic modulus and the elastic/plastic deformation behaviour parameters in a relatively easy fashion. If the nanohardness values decrease with the increase of applied indentation test load, such phenomenon is known as indentation size effect (ISE) [7, 9, 10]. On the other hand, the reverse indentation size effect (RISE) means

that micro/nanohardness value increases with increasing applied indentation load [8, 11]. ISE or RISE behavior of materials show where, when, and to what extent the materials can be used.

Mg-Al-Zn alloys, named as AZ series, and AZ63 in particular, are some of the extensively used magnesium alloys. On the other hand, mechanical properties of these series are quite weak [12]. Thus, in this study we have aimed to produce AZ63 magnesium alloys containing different CaO content, to investigate the nanohardness behaviour of these alloys. In the literature, in recent studies, an improvement in the mechanical properties of magnesium alloys was observed with small CaO additions [13]. However, according to our best knowledge, there are no reports on the production by mechanical alloying and mechanical properties of the AZ63 magnesium alloys having different CaO content. Additionally, nanoindentation deformation behaviour of the AZ63 was reported by analyzing the nanoindentation load-displacement curves.

## 2. Experimental procedure

In this study AZ63 magnesium alloys were produced by mechanical alloying technique. AZ63 magnesium alloys with different amounts of CaO (Table I) were fabricated from high purity powders Mg (ABCR, 99.9% purity), Zn (ABCR, 99.9% purity), Al (MERC, 98% purity), Si (ALDRICH, 99% purity), CaO (BDH, 99% purity). Stearic acid was used (2%) as process control agent. Powders were mixed in a steel grinding bowl in argon atmosphere. A Fritsch-pulversitte 7 planetary milling instrument was used for alloying process. Milling time was set to 6 hours with a speed of 600 rpm. Samples were taken from the grinding bowls by opening in a glove-box. Stearic acid was evaporated by an-

\*corresponding author; e-mail: [sduosman@gmail.com](mailto:sduosman@gmail.com)

TABLE I

Chemical composition of the alloys (mass%).

Sample name	Al	Zn	Si	CaO concentration	Mg
AZ63	2.7	6.0	0.3	0.0	Bal.
AZ63-0.1CaO	2.7	6.0	0.3	0.1	Bal.
AZ63-0.3CaO	2.7	6.0	0.3	0.3	Bal.
AZ63-0.5CaO	2.7	6.0	0.3	0.5	Bal.

nealing in an atmosphere-controlled oven at 380 °C for 1 hour. XRD (RIGAKU Smart Lab) and SEM analysis were performed on powder samples. Powder samples were converted to pellets by pressing in a steel mold with 1 cm diameter. During pressing first 1500 kg, and then 6500 kg load was applied for 10 minutes. Samples were sintered by annealing in an atmosphere-controlled oven at 430 °C for 3 hours. Finally, samples were moulded and polished with 800 grid and 4000 grid abrasive papers. Nanohardness analysis was performed on moulded and polished samples using a Hysitron TI-950 Triboindenter with a Berkovich tip. Nanoindentation load-displacement curves were analyzed by most common Oliver-Pharr [14] method. The nanohardness is defined as,

$$H_{\text{nano}} = \frac{P_{\text{max}}}{A}, \quad (1)$$

where  $P_{\text{max}}$  is the maximum test load and  $A$  is the projected contact area at  $P_{\text{max}}$ . For a perfect Berkovich indenter the projected contact area is given by

$$A_c = 24.5h_c^2, \quad (2)$$

where  $h_c$  is contact depth. For an easier interpretation of nanohardness behaviour at various depths, the maximum load was changed at regular intervals to 1000, 2000, 3000, 4000, 5000, and 6000  $\mu\text{N}$  under a loading/unloading rate of 1200  $\mu\text{N s}^{-1}$ , and the load was held at each maximum value for 2 s. For a particular load, at least five indentation tests were conducted on the sample surface to increase the reliability of the experimental results.

### 3. Results and discussion

Figure 1 shows the representative applied indentation test load-penetration depth curves for all examined materials. For each record these curves were analyzed using the aforementioned Oliver-Pharr procedure. These curves demonstrate a smooth shape, and no pop-in could be detected. Elastoplastic behaviour of these alloys can be clearly seen in this figure. The unloading curves show the similar behavior if they are shifted according to their final depths. Thus we can also say that these alloys have similar deformation mechanism for our indentation test load range. As we can see from the scanning probe microscope micrograph of AZ63 alloys (Fig. 1), the sample surfaces are homogeneous and without cracks. Surface roughness values are given in Table II. Furthermore, we believe that there is no significant surface finishing effect since the shape of the Berkovich indenter, given in the inset of Fig. 1, is exactly the same as the indentation observed on the sample surface.

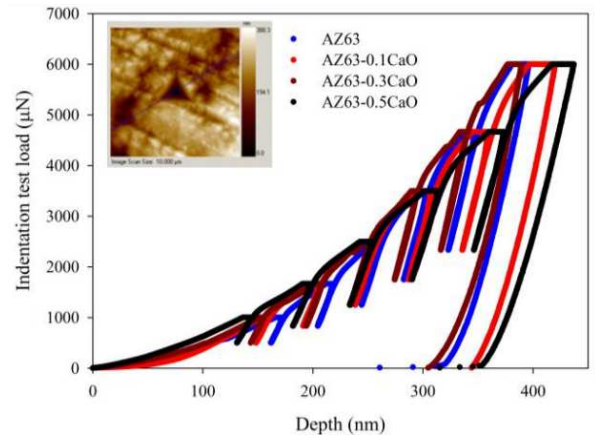


Fig. 1. Indentation test load versus depth graph of AZ63 alloys.

TABLE II

Crystallite size of the alloys as a function of CaO doping concentration.

Sample name	Average particle size [ $\mu\text{m}$ ]	Average crystallite size ( $D$ ) [ $\text{nm}$ ]	Load independent nanohardness [ $\text{GPa}$ ]	Average roughness ( $R_a$ ) [ $\text{nm}$ ]
AZ63	17	49.85	$1.55 \pm 0.016$	67.354
AZ63-0.1CaO	8	35.34	$1.64 \pm 0.022$	62.436
AZ63-0.3CaO	13	24.32	$1.61 \pm 0.018$	64.228
AZ63-0.5CaO	22	20.83	$1.36 \pm 0.024$	74.954

Morphological investigation plays an important role in determination of surface properties and nature of the materials. SEM images of these alloys, having different CaO concentrations, are shown in Fig. 2. The images also show that the surfaces are homogenous and densely packed. The average particle size of the alloy without CaO addition, which was measured by a pixel analyzing program, was about 17  $\mu\text{m}$  (Fig. 2a). On the other hand the dimensions of the particles were decreased with CaO addition and surface of the alloys became smoother than that of the alloys without CaO addition. Surface roughness values have decreased with the increasing CaO content up to 5% (Table II). Average particle size values of these alloys are 17, 8, 13 and 22  $\mu\text{m}$  for AZ63, AZ63-0.1CaO, AZ63-0.3CaO and AZ63-0.5CaO, respectively. It is observed from the SEM images that the particle size of these alloy structures have decreased with CaO content up to 5%, and then have increased for higher CaO concentration. From the SEM images, we could see that low content of CaO can improve the matrix microstructure and particle size. With the addition of 0.1 and 0.3% of CaO, the particle size has decreased. With the addition of 0.6% of CaO the particle size has increased and the coarsening of particles has become obvious.

In order to investigate the structural properties, the XRD analysis of pure and CaO-doped AZ63 magnesium alloys was employed. Figure 3 shows XRD pattern of the alloys having different CaO concentrations.

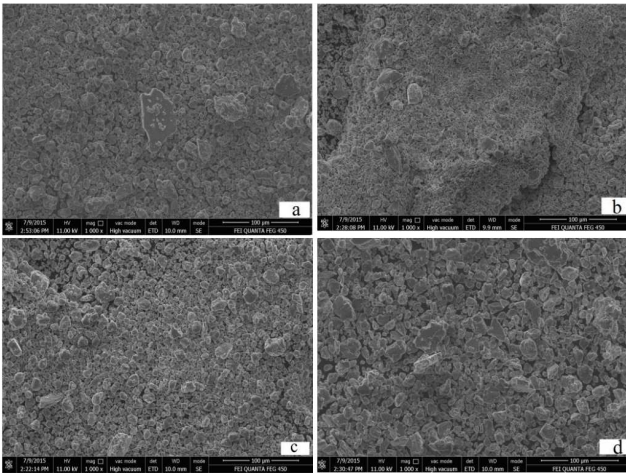


Fig. 2. SEM images of (a) AZ63, (b) AZ63-0.1CaO, (c) AZ63-0.3CaO, (d) AZ63-0.5CaO.

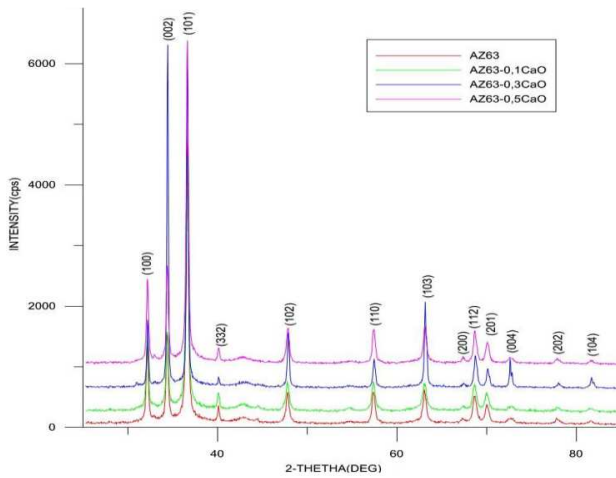


Fig. 3. XRD pattern of AZ63 alloys.

XRD pattern shows that preferred orientations are (100), (002) and (101). Average crystallite size was calculated using Scherrer formula [15].

$$D = \frac{0.94\lambda}{\beta \cos \theta}, \quad (3)$$

where  $\lambda$  is the wavelength of X-ray radiation and  $\theta$  is the Bragg's angle of the corresponding peak. The calculated average crystallite sizes of the alloys are given in Table II. The sample containing 0.1% of CaO has been shown to have a decreased particle size. It is found that samples containing 0.3% and 0.5% of CaO show an increase in the particle sizes. The average particle sizes of the samples are given in Table II. It is well known that any defect in regular crystal structure or grain boundaries obstruct the dislocation, which makes plastic deformation more difficult. Thus, one can say that the greater the grain boundary density or crystal defects are, the greater are the hardness values. Smaller particle size creates more grain boundaries, and consequently, affects the nanohardness properties of the materials. It can be seen from the Table II that particle size of AZ63 decreases

when the amount of CaO is 0.1% and 0.3%. However it increases for 0.5% of CaO content.

Figure 4 shows the variation of nanohardness as a function of test load. From the figure, one can see that nanohardness values increase with increasing test load, with the exception of AZ63-0.5CaO sample. In this sample the nanohardness values decrease with the increasing test load. The curves in Fig. 4 show a non-linear behaviour of nanohardness values up to a certain value of test load, after which the nanohardness tends to achieve saturation. This type of behaviour called indentation size effect [7, 9, 16] for the AZ63-0.5CaO sample and for the other samples it is called reverse indentation size effect [8, 11].

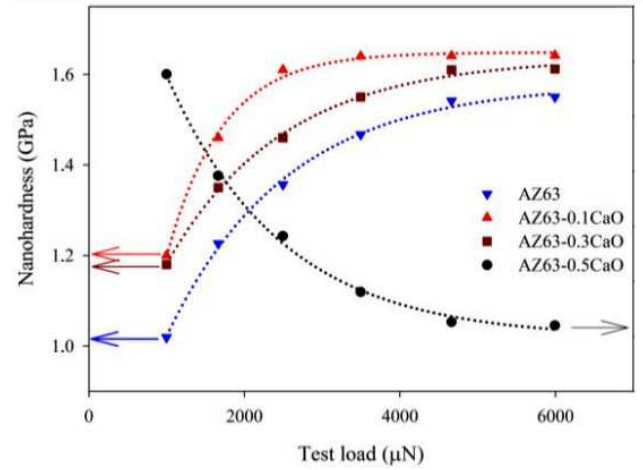


Fig. 4. Nanohardness variation as a function of test load.

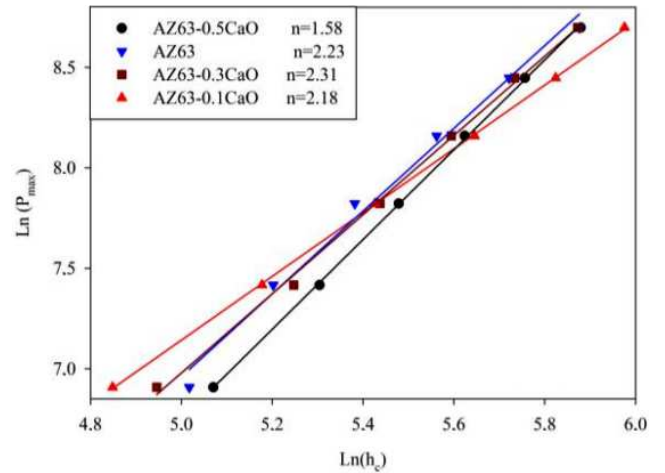


Fig. 5. Plots of  $\ln(P_{\max})$  vs.  $\ln(h_c)$  according to the Meyer law.

The existence of the RISE or ISE makes it difficult to report hardness value measured at a single load level for material characterization. A complete evaluation of the hardness characteristics for a given material needs further knowledge of the cause of the non-linear behaviour

and a load-independent hardness. ISE and RISE were reported in the literature for a variety of materials [8, 16]. The relationships between the contact depth and the indentation test load has been proposed in the following manner:

$$P_{\max} = Kh_c^n, \quad (4)$$

where power index  $n$  is the Meyer number and  $K$  is hardness constant. The  $K$  and  $n$  values in Eq. (4), given in Table II and below, can be obtained from the  $\ln(P_{\max})$  vs.  $\ln(h_c)$  graph (Fig. 5). For normal ISE behaviour, the exponent  $n < 2$ . When  $n > 2$ , there is a reverse ISE behaviour. According to the definition of the apparent hardness (Eq. (1)), no ISE would be observed for  $n = 2$ . Observed  $n$  values are 2.23, 2.18, 2.31, 1.58 for AZ63, AZ63-0.1CaO, AZ63-0.3CaO and AZ63-0.5CaO, respectively. The decrease of nanohardness for  $n < 2$  and increase for  $n > 2$ , as the test load increases, are in good agreement with other reported results [11, 16].

From the Fig. 4 nanohardness test load plots can be divided into two stages. In the first stage, nanohardness increases to a maximum value, with the exception of the AZ63-0.5CaO alloy. In the second stage it holds at a constant value (saturation region) at around 5000  $\mu\text{N}$ . That is, no matter how much load over 5000  $\mu\text{N}$  is applied to the AZ63 alloys, changes in the nanohardness value will be insignificant. These indicate that hardness value depends on applied indentation test load and there is a relation between the indentation test load and size of the indenter. The increase in hardness at small penetration depth is usually attributed to the transition between purely elastic to elastic/plastic contact and at this stage the nanohardness is not accurately measured by the mean contact pressure. Only under the condition of a fully developed plastic zone, does the mean contact pressure represent the nanohardness. When there is no plastic zone, or with only partially formed plastic zone, the mean contact pressure is less than the nominal hardness [14]. After the first stage, 5000  $\mu\text{N}$ , at high indentation test load, the nanohardness reaches a constant value (Fig. 5) in all examined alloys, which could be regarded as an intrinsic property of these materials.

In addition, in the literature, Quinn and Quinn [17] have examined the variation of Vickers microhardness with indentation load for a variety of ceramic materials. They have observed that their hardness load curve exhibits obvious transition to plateau of constant hardness and they concluded that the transition in such curve corresponds to the intrinsic hardness value of the material. In this study, this plateau is reached at approximately 5000  $\mu\text{N}$  of applied test load, for studied alloys.

As it is evident from the Fig. 4, the nanohardness after 5000  $\mu\text{N}$  remains nearly constant with small fluctuation, possibly associated with dislocation activities. Therefore we can say that the intrinsic nanohardness values are 1.55, 1.64, 1.61 and 1.36 GPa for AZ63, AZ63-0.1CaO, AZ63-0.3CaO and AZ63-0.5CaO, respectively. Same hardness behavior can be seen in various thin films [18] and magnesium alloys [19].

## 5. Conclusions

In conclusion, authors have presented the first report on the nanohardness properties of CaO-doped AZ63 magnesium alloys. These alloys were successfully produced by mechanical alloying under argon atmosphere. Analysis of the results led to the following conclusions:

1. Nanohardness experimental results of the AZ63 magnesium alloys show peak load dependence. Nanohardness values of all samples increase with the increasing test load, with the exception of AZ63-0.5CaO sample. In this sample the nanohardness value decreases with the increasing test load.
2. It is observed from the SEM images and XRD patterns that the particle sizes of the alloys structures have increased with CaO content up to 5% and then also increased for the higher levels.
3. Nanohardness properties of AZ63 biomaterials can be controlled and calibrated by adjusting the CaO concentrations.

## Acknowledgments

The financial support from research foundation of Mustafa Kemal University (grant no. 11580) is gratefully acknowledged. This work is partially supported by the Scientific and Technological Research Council of Turkey (TUBITAK) with Grant No. 213M699, and the Turkish State Planning Organization (DPT) with Project no. 2010K121220.

## References

- [1] R. Gradinger, P. Stolfig, *Magnesium Technology* **2003**, 231 (2003).
- [2] M.O. Pekguleryuz, E. Baril, P. Labelle, D. Argo, *J. Adv. Mater-Covina* **35**, 32 (2003).
- [3] C.L. Liu, Y.C. Xin, G.Y. Tang, P.K. Chu, *Mat. Sci. Eng. A* **456**, 350 (2007).
- [4] W. Zhang, M. Li, Q. Chen, W. Hu, W. Zhang, W. Xin, *Mater. Design* **39**, 379 (2012).
- [5] H. Jafari, M. Idris, A. Ourdjimi, G. Payganeh, *Acta Metallurgica Sinica (English Letters)* **22**, 401 (2009).
- [6] M.L.B. Palacio, B. Bhushan, *Mater. Charact.* **78**, 1 (2013).
- [7] A.E. Ozmetin, O. Sahin, E. Ongun, M. Kuru, *J. Alloys Compd.* **619**, 262 (2015).
- [8] E. Yücel, O. Şahin, *Ceram. Int.* **42**, 6399 (2016).
- [9] O. Sahin, O. Uzun, M. Sopicka-Lizer, H. Gocmez, U. Kölemen, *J. Phys. D* **41**, 035305 (2008).
- [10] O. Sahin, O. Uzun, U. Kolemen, N. Ucar, *Mater. Charact.* **59**, 729 (2008).
- [11] H.S. Guder, E. Sahin, O. Sahin, H. Gocmez, C. Duran, H.A. Cetinkara, *Acta Phys. Pol. A* **120**, 1026 (2011).

- [12] A. Incesu, A. Gungor, *Adv. Mater. Process. Technol.* **1**, 243 (2015).
- [13] S.-H. Ha, J.-K. Lee, S.K. Kim, *Mater. Trans.* **49**, 1081 (2008).
- [14] W.C. Oliver, G.M. Pharr, *J. Mater. Res.* **7**, 1564 (1992).
- [15] P. Zavalij, *Fundamentals of powder diffraction and structure characterization of materials*, Springer Science Business Media, NY 2005.
- [16] O. Sahin, O. Uzun, M. Sopicka-Lizer, H. Gocmez, U. Kölemen, *J. European Ceram. Soc.* **28**, 1235 (2008).
- [17] J. Quinn, G.D. Quinn, *J. Mater. Sci.* **32**, 4331 (1997).
- [18] I. Karaca, O. Uzun, U. Kölemen, F. Yılmaz, O. Şahin, *J. Alloys Compd.* **476**, 486 (2009).
- [19] S. He, L. Peng, X. Zeng, W. Ding, Y. Zhu, *Mater. Sci. Eng. A* **433**, 175 (2006).